Localized Nanoscopic Surface Measurements of Nickel-Modified Mica for Single-Molecule DNA Sequence Sampling

Carlin Hsueh,[†] Haijian Chen,[‡] James K . Gimzewski,[†,§,⊥] Jason Reed,[*,§] and Tarek M. Abdel-Fattah[*,∥]

Department of Chemistry and Biochemistry, University of California—Los Angeles, 607 Charles Young Drive East, Los Angeles, California 90095, United States, Department of Physics, College of William and Mary, Williamsburg, Virginia 23185, United States, UCLA California NanoSystems Institute (CNSI), 570 Westwood Plaza, Los Angeles, California 90095, United States, Applied Research Center, Jefferson National Laboratory and Department of Biology, Chemistry and Environmental Science, Christopher Newport University, Newport News, Virginia 23606, United States, and International Center for Materials Nanoarchitectonics Satellite (MANA), National Institute for Materials Science (NIMS), Tsukuba 305-0047, Japan

ABSTRACT Cleaved, cation-derivatized Muscovite mica is utilized extensively in atomic force microscopy (AFM) imaging because of its flatness over large areas (millimeter cleavage planes with local root-mean-square roughness < 0.3 nm), ease of preparation, and ability to adsorb charged biomolecules such as DNA (work by Hansma and Laney, Guthold et al., and McMaster et al.). In particular, $NiCl_2$ treatment has become a common method for controlling DNA adsorption on mica substrates while retaining the mica's ultraflat surface (work by Pietrement et al.). While several studies have modeled the mica/metal ion/DNA system using macroscopic colloidal theory (DLVO, etc.; Pietrement et al., Sushko et al., Pastre et al., and Cheng et al.), nickel/mica's physicochemical properties have not been well characterized on the nanoscale. Efforts to manipulate and engineer DNA nanostructures would benefit greatly from a better understanding of the surface chemistry of nickel/mica. Here we present in situ nanometer- and attogram-scale measurements and thermodynamic simulation results that show that the surface chemistry of nickel-treated mica is more complex than generally appreciated by AFM practitioners because of metal-ion speciation effects present at neutral pH. We also show that, under certain preparations, nickel/mica allows in situ nanoscopic nucleotide sequence mapping within individual surface-adsorbed DNA molecules by permitting localized, controlled desorption of the double helix by soluble DNA binding enzymes. These results should aid efforts to precisely control the DNA/mica binding affinity, particularly at the physiological pH ranges required by enzymatic biochemistry (pH 7.0—8.5), and facilitate the development of more complex and useful biochemical manipulations of adsorbed DNA, such as single-molecule sequencing.

KEYWORDS: single-molecule DNA sequencing • surface-modified mica • ToF-SIMS • AFM and surface analysis

INTRODUCTION

Engineered planar substrates, such as chemically derivatized glass, silicon/silicon oxide, and gold/thiol-based self-assembled monolayers (SAMs) are critical enabling components in widely used and commercially important technologies such as "next gen" DNA sequencing (9, 10), nucleic acid microarrays (11), and surface-plasmon-resonance biosensors (Biacore, etc.) (12). Because most of these technologies employ far-field optical microscopy or photonic detection, surface topography and nanometer-scale variations in the surface chemistry of the substrate are not of concern. However, in scanning probe microscopy of nucleic acids and nucleic acid/protein complexes, substrate surface topography and local physicochemical properties are critical issues. When used with the proper attention to substrate/sample preparation, scanning probe microscopy offers substantial advantages over photonic detection in terms of sensitivity (no labels), resolution (submolecular-to-atomic), and breadth of measurement modalities (topography, stiffness, adhesiveness, and thermal and electrostatic properties). Paradoxically, substrates used in scanning probe microscopy tend to be less engineered and less well characterized than are scaffolds and surfaces used in systems with photonic detection. This is particularly true in the of study of biopolymers, such as DNA and protein fibers of various kinds, which can be micrometers-to-millimeters in length and thus require vast areas of atomically flat surface that can be very difficult to achieve on chemically modified glass or gold/thiol/SAM substrates. Freshly cleaved mica complexed with multivalent cations is a very popular but simple system used to bind DNA for atomic force microscopy (AFM) imaging in liquid and in air. In particular, Ni^{2+} ion, applied in the form of an aqueous chloride or nitrate

* To whom correspondence should be addressed. E-mail: Fattah@cnu.edu (T.M.A.-F.), jreed@cnsi.ucla.edu (J.R.).
Received for review August 5, 2010 and accepted October 12, 2010
† University of California—Los Angeles.
‡ College of William and Mary.
§ UCLA California NanoSystems Institute.
∥ Christopher Newport University.
⊥ International Center for Materials Nanoarchitectonics Satellite.
DOI: 10.1021/am100697z

salt solution, has been shown to produce unusually strong DNA adsorption on mica compared to similar divalent metal ions, and this has been used to advantage in a number of studies, including our own (13), where strong adsorption is required (1, 4). Despite nickel/mica's widespread use by the AFM community and its potential as a substrate for DNA nanotechnologies of various kinds, knowledge of its nanoscale physicochemistry is limited.

A series of classic studies used a surface force apparatus (SFA) to study the interaction between two cleaved mica surfaces in various mono- and divalent aqueous metal-ion electrolytes (14, 15) (though not including Ni^{2+}). These authors analyzed the mica−mica interaction in terms of an extended Derjaguin−Landau−Verwey−Overbeek (DLVO) theory of colloid stability. Notably, their experiments were mostly conducted at pH 5.8. Workers studying the biochemistry of single DNA molecules bound to mica with AFM have extended this classic SFA-based work, using a generalization of the DLVO theory to model the force interaction of a charged DNA molecule and mica surface, rather than two mica surfaces, in aqueous metal-ion electrolytes at physiological pH (7.0−8.5) (4, 5, 7, 8). However, metal ions in solution are known to exhibit complex speciation behavior (16), and this important aspect of metal-ion chemistry has not been taken into account in the past modeling and discussion of DNA binding to mica. Further, the nickel-ion-treated mica surface itself has not been directly characterized because of the minute quantities of material involved.

In this report, we use a combination of nanoscale analytical techniques to probe the properties of nickel/mica on the molecular scale. We employ an exquisitely sensitive surface analysis technique, secondary-ion mass spectrometry, to confirm in situ partial ion exchange between Ni^{2+} in the solution and native K^+ present on the untreated mica surface. Using AFM, we show that a smooth, stable, but difficult-to-detect molecular monolayer can form on mica treated with aqueous $NiCl_2$ at pH ~7, likely a result of metal or metal hydroxide precipitates. Importantly, this result indicates that the actual substrate−molecule interaction can be mediated in some cases by a molecular adlayer of physicochemical properties different from those of the mica itself. We present thermodynamic simulations that show that nickel-ion speciation in aqueous solutions is highly sensitive to pH in the range 6−8. As a consequence, the solution concentration of the divalent species can vary widely from what is assumed, and the speciation of other metal-ion complexes can be unpredictable unless great care is taken to stabilize the pH condition and redox condition of the solution. Taken together, our simulation and experimental results strongly suggest that more detailed modeling and experiments are needed to properly understand and control the mica/metal ion/DNA system at physiological pH. In order to determine the biofunctional characteristics of the nickel/mica surfaces, we digested mica-adsorbed plasmid DNA with a restriction enzyme, *RsaI*. We show that nickel/mica is compatible with enzymology conducted directly on the surface-fixed DNA molecules and can be used to precisely locate DNA sequence motifs within single molecules (17). Similarly, it has potential uses as a scaffold or substrate for engineering DNA nanostructures and in other areas of DNA nanotechnology, like single-molecule DNA sequencing.

RESULTS AND DISCUSSION

In Situ Time-of-Flight Secondary-Ion Mass Spectrometry (ToF-SIMS) of Ni^{2+}/Mica. We used ToF-SIMS to probe elemental properties in the first few atomic layers of the nickel-derivatized mica surface. ToF-SIMS uses energetic primary ions to probe the sample surface. As a result of the impact, secondary ions are generated from a close vicinity (a few angstroms) of the impinging point on the sample and are collected for deducing chemical information. These secondary ions usually come from the top couple of atomic layers. In ToF-SIMS, the primary ion is pulsed and only a small dose (less than 10^3 ions cm^{-2}) of primary ions is delivered to the sample surface during the entire process; thus, only a small fraction of the top surface layer is impacted, and the rest is essentially intact. Furthermore, the primary ion beam can be focused to a submicrometer-sized spot and scanned across the sample, generating a spatial mapping of the surface elemental composition. As such, it is an ideal tool for characterizing the quantity and distribution of nickel adsorbates on the mica surface.

Spectra from Untreated and Treated Silicon Wafer Samples. We took ToF-SIMS spectra from the surface of nickel-treated silicon wafers, for reference. The positive spectra for the blank silicon wafer and $NiCl_2$-solution-treated silicon wafer look very similar at a glance, as shown in the plots below. Plots a and b of Figure 1 show a range from *m/z* 0 to 100 for blank and treated silicon wafers. Plots c and d of Figure 1 show a zoom in view in the range *m/z* 57.5−60.5. Close examination reveals that the blank silicon wafer does not carry a Ni^+ signal, while the treated silicon wafer does. The relative abundance of ^{58}Ni and ^{60}Ni isotopes observed closely matches the naturally occurring ratio of 0.68:0.26. Notice that the nickel signal is not dominant in the spectrum of a $NiCl_2$-treated silicon wafer, which may indicate that the treatment does not introduce excessive nickel on the sample surface. The peaks in Figure 1c,d represent the two nickel isotopic peaks, and other peaks represent hydrocarbons due to surface contamination. For the negative spectra (not shown) on the silicon wafers, Cl^- shows up in the both untreated and treated silicon wafers, but the treated silicon wafer has a higher relative Cl^- content. While there are Cl^- ions in the untreated silicon wafer spectrum, most likely due to salt intrinsic to the wafer itself, on the treated silicon wafer, the relative intensity of $^{35}Cl^-$ to Si^- (or $^{35}Cl^-$ to CN^-) is approximately 6 times that of the untreated silicon wafer.

Spectra from Untreated and Treated Mica Samples. Both untreated and treated mica samples were mounted with a metal grid to help produce an effective extraction field, and during acquisition, electron charge neutralization was used. Figure 1 shows the typical spectra for blank mica (e) and $NiCl_2$-solution-treated mica (f) in a

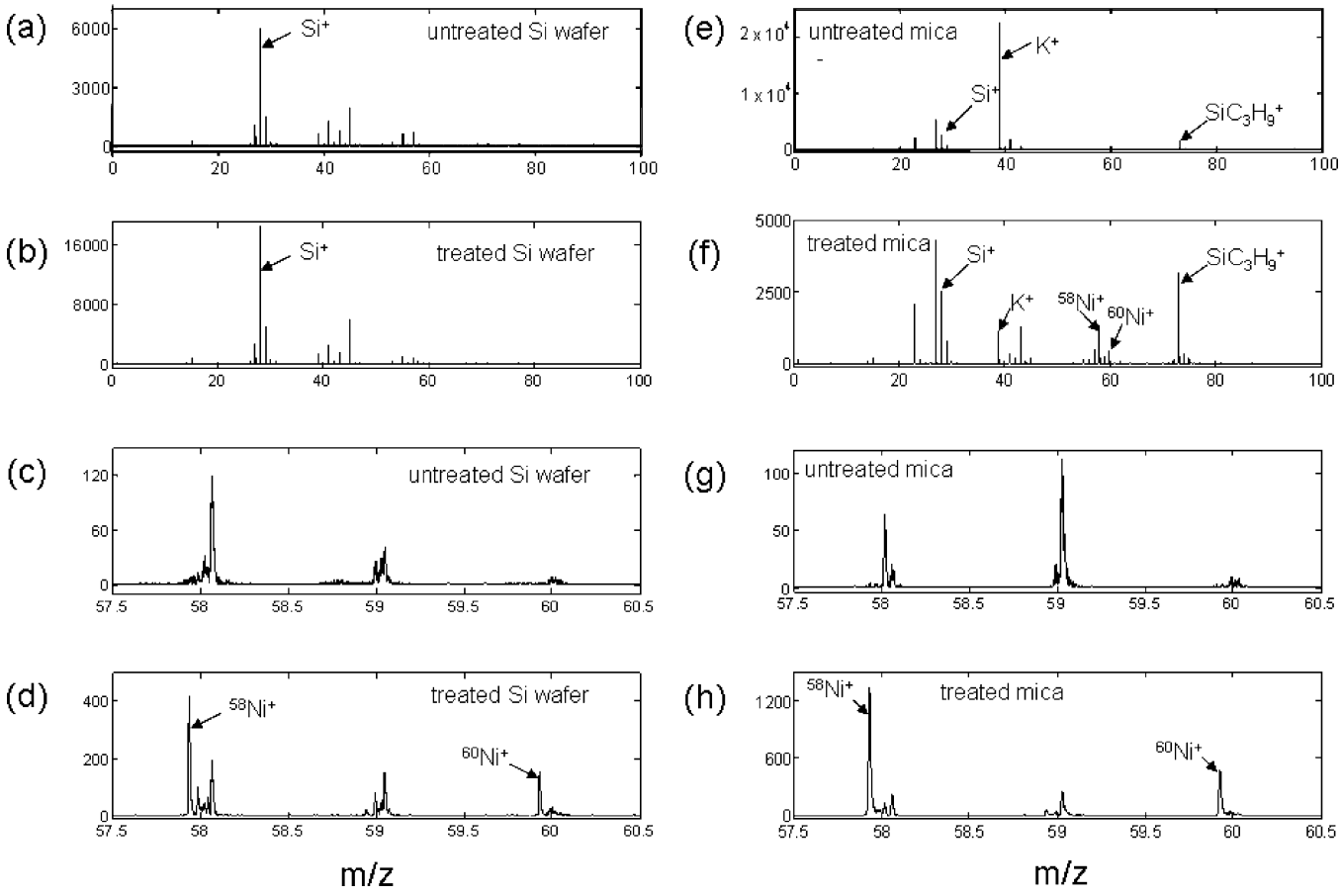

FIGURE 1. ToF-SIMS spectra (a and c) for untreated silicon wafers, (e and g) for untreated mica, (b and d) for nickel-treated silicon wafers, and (f and h) for nickel-treated mica.

range from *m/z* 0 to 100. It is apparent that the untreated mica has a relatively higher K^+ signal (K^+:$Si^+ \sim 7.6$:1) and does not have Ni ions. Meanwhile, the $NiCl_2$-solution-treated mica does show Ni^+ ion signals, accompanied by an approximately 19-fold-reduced K^+ signal versus the untreated signal (K^+:$Si^+ \sim 0.4$:1). Plots g and h Figure 1 of show a zoom in view in the range *m/z* 57.5−60.5. The negative spectra (not shown) for both samples Cl^- peaks, but the relative intensity is almost doubled for treated mica. For the blank, $^{35}Cl^-$:$CN^- \sim 1.2$ ($^{35}Cl^-$:$Si^- \sim 0.2$), while in the treated mica, $^{35}Cl^-$:$CN^- \sim 2.2$ ($^{35}Cl^-$:$Si^- \sim 0.4$).

Mapping the Spatial Uniformity of the Nickel Adlayer to Submicrometer Resolution. Figure 2 shows the mapping of silicon and nickel fragments from a mica surface treated with a nickel solution. Because the mica surface contains −OH groups, the intensity of the silicon fragments is directly proportional to the distribution of the ion-exchange sites for nickel ions. Figure 2 indicates an even distribution of nickel with no agglomeration.

AFM Measurements of Ni^{2+}/Mica Surface Roughness. The Ni^{2+}-treated mica surfaces were flat, uniform, and stable and can be used for DNA imaging. Figure 3 shows representative images, with cross-sectional profiles, from samples treated with water (a) or 10 mM $NiCl_2$ (b). The average surface roughness of the sample treated with water is 0.20 nm or less, peak-to-peak, while the 10 mM $NiCl_2$-treated sample is slightly rougher, 0.30 nm peak-to-peak,

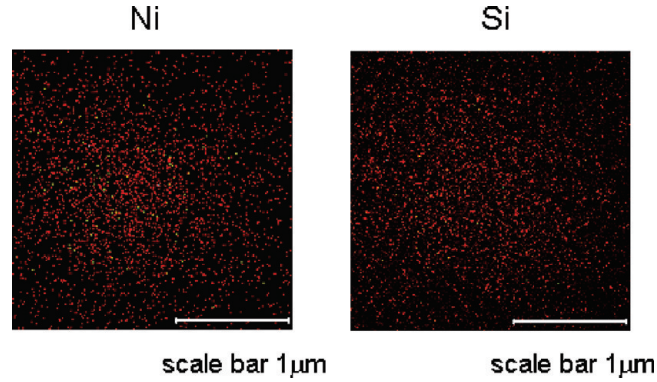

FIGURE 2. ToF-SIMS images showing the distribution of silicon and nickel on the mica surface.

and is mottled in appearance. In order to determine the effect of the $NiCl_2$ solution concentration on the surface roughness, samples were prepared using the standard procedure, with $NiCl_2$ concentrations varying from 0 to 10 mM (Figure 4a). There is an obvious difference between the apparent surface roughness without and with $NiCl_2$, while within experimental error the roughness is independent of the $NiCl_2$ concentration at both pH 7.1 and 5.1. The effect of the pH of the $NiCl_2$ solution (10 mM) on the preparation is presented in Figure 4b. We found no significant difference in roughness between surfaces prepared from solutions with pH 3.0, 3.6, 5.1, 7.0, or 7.3. We note that the increase in the apparent surface roughness caused by $NiCl_2$ treatment

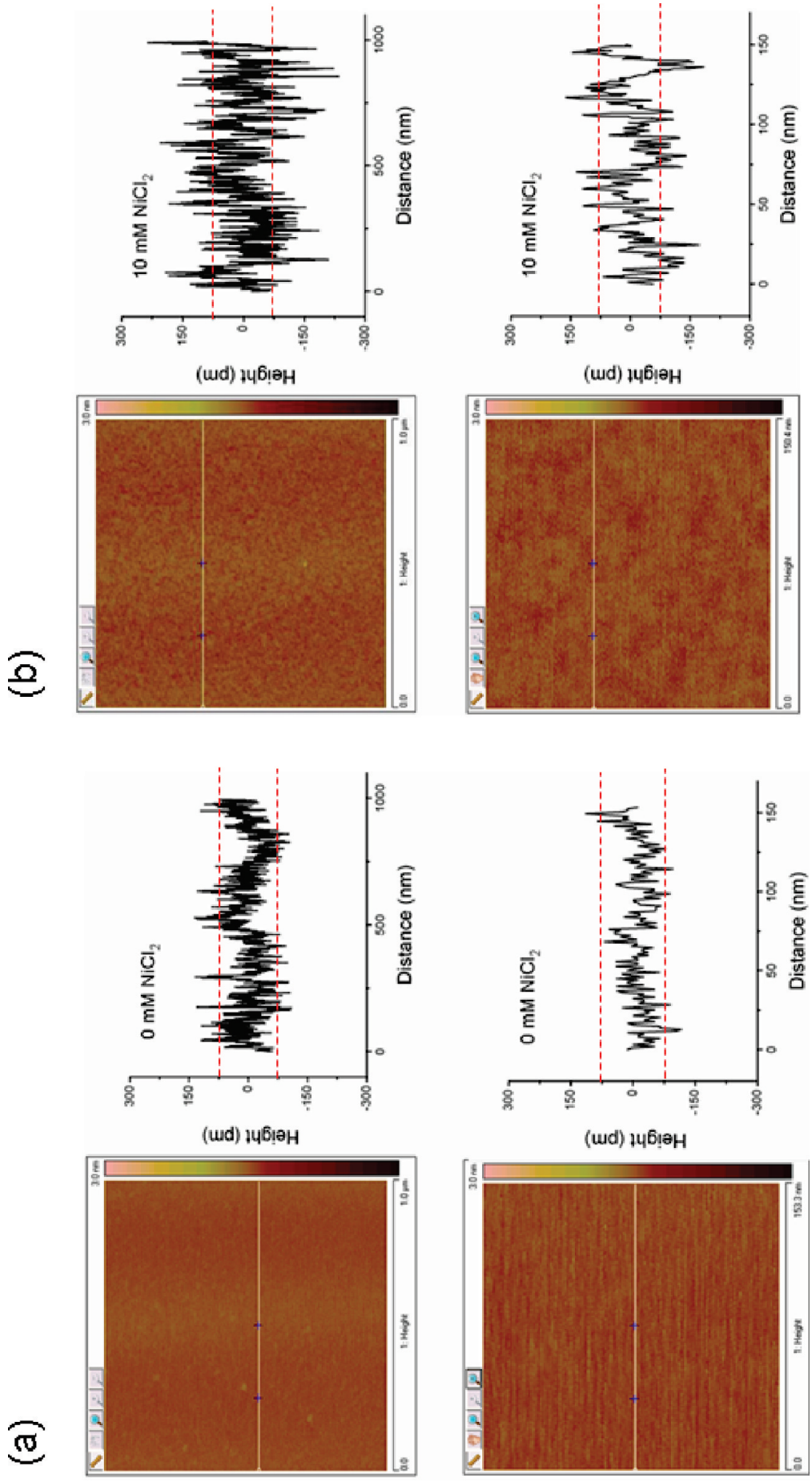

FIGURE 3. Typical surface cross sections of (a) 0 mM and (b) 10 mM $NiCl_2$ deposited on mica. Dashed red lines at ± 100 pm are for reference.

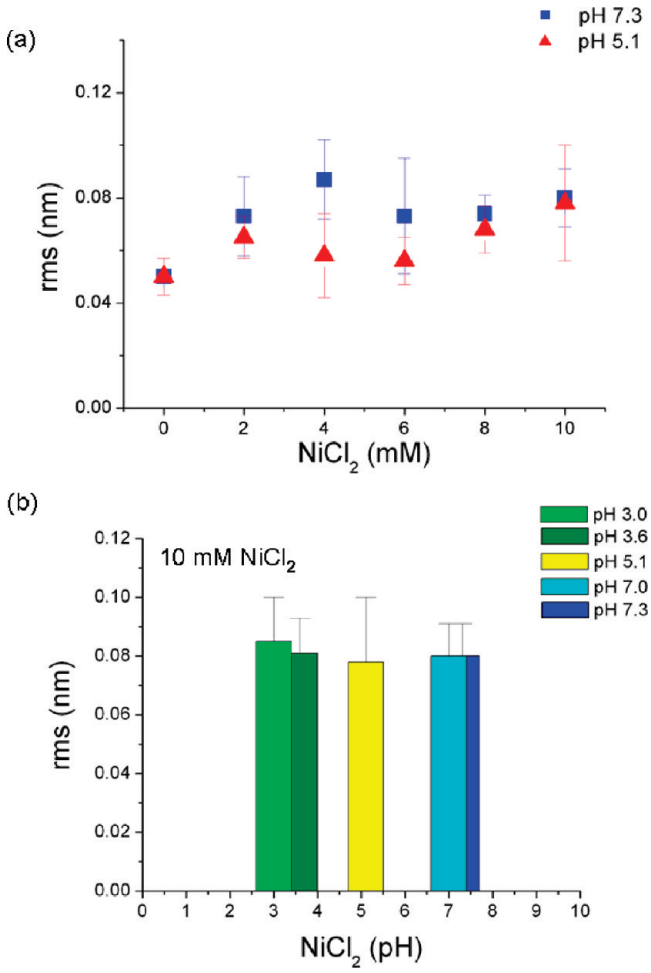

FIGURE 4. (a) Surface roughness of $NiCl_2$-treated mica as a function of the $NiCl_2$ concentration. (b) Surface roughness of mica treated with 10 mM $NiCl_2$ solutions, at solution pH from 3.0 to 7.3.

may be caused by several factors in addition to pure geometrical effects, including ion adsorption onto the AFM tip, the change in the ion-mediated van der Waals, and potentially strong electrostatic interactions between nickel ions adsorbed onto a mica surface and the AFM tip.

Thermodynamic Simulation of Aqueous Nickel-Ion Speciation. In an effort to further understand the origin of the surface roughness observed with AFM, we conducted thermodynamic modeling of the chemical system containing Ni^{2+} ions in aqueous solutions. All of the thermodynamic modeling calculations refer to the bulk solutions only. The different phase formations under a closed system and/or surrounding conditions can be calculated from the changes of the free energy, ΔG, of the reaction under given conditions. In the thermodynamic modeling of the aqueous Ni^{2+} ions, we define the system to be investigated by the following main components: Ni^{2+}, $NiCl^+$, $NiCl_2$, $Ni(OH)^+$, $Ni(OH)_2$, $Ni(OH)_3^-$, and $Ni(OH)_4^{2-}$. Figure 5a shows that concentrations of all possible nickel species can be formed at different pHs. As shown in Figure 5b, the Ni^{2+} ions form weak complexes with Cl^- ions in the acidic pH range. However, with an increase in the pH, Ni^{2+} ions form stable solid precipitates of $Ni(OH)_2$ in the pH range of 7−14. On the basis of thermodynamics modeling, the pH range of 6−8 can produce many nickel species, which may lead to inconsistent surface chemistry and nonuniform DNA binding between replicate preparations. A pH below 6 is the optimum pH for introducing nickel species to the mica surface. Interestingly, the pH does not appear to change the roughness of the samples under the conditions used here. This indicates that while the surface layer associated with $NiCl_2$ may be in the form of nickel hydroxide, there is no large change in the deposition properties above pH 6, as is suggested by our thermodynamic simulation.

In Situ Detection of the Nucleotide Sequence in Adsorbed DNA Molecules. In order to determine the biofunctional characteristics of the nickel/mica surfaces, we elongated, fixed, and in situ digested plasmid DNA with a restriction enzyme, *RsaI*. *RsaI* recognizes a four-nucleotide sequence, GTAC, and cleaves both strands of the double helix at that location in the molecule, assuming that the chemical environment allows the enzyme to function normally. In this system, both the conformation of the adsorbed DNA and the enzyme cleavage kinetics can give qualitative information about the fate of nickel bound to the substrate and the strength of the DNA−mica interaction.

Figure 6 shows a typical image, with two linearized pUC19 molecules elongated on a $NiCl_2$-treated mica surface and then digested in an aqueous salt buffer for 30 min at 37 °C. AFM images were taken from dried samples directly. Height profiles taken along the backbone contour of the molecules show depressions corresponding to the locations of the GTAC sequence sites predicted from the known sequence of pUC19. PUC19 has two *RsaI* recognition sites, and upon complete digestion, fragments of 75, 223, and 584 nm are produced (assuming 0.33 nm per bp of B-DNA). Because of attractions between the DNA molecule and the Ni^{2+} surface, fragments remain adhered to the surface in their original order within the DNA molecule. The Ni^{2+} adheres the DNA to the surface but loosely enough so that the ends at the gap sites have flexibility to move either during enzyme incubation or during postdigestion washing. This property results in "swinging" ends that enlarge gaps produced by enzyme cleavages. Proteins can also adhere to the nickel/mica surface, although with less avidity than the charged DNA molecule, as can be seen in Figure 6, where *RsaI* enzymes surround digested pUC19.

In our experiments, a majority of the plasmid molecules on the surface remained in an elongated, nonequilibrium conformation, through the entire digestion, washing, and drying process. It has been established that DNA molecules bound loosely to mica will relax to a random conformation in the 2D plane indicative of nearly free diffusion in the plane, even while apparently remaining confined to the surface (8). Clearly, in this case, the DNA are bound to the nickel/mica strongly enough to resist entropic relaxation. However, typically 30−40% of the recognition sites available are cleaved (see the Methods section). This indicates that the adsorbed molecules retained enough local conformational flexibility to permit the enzyme to dimerize, encircle the double helix, and access the bases via the DNA

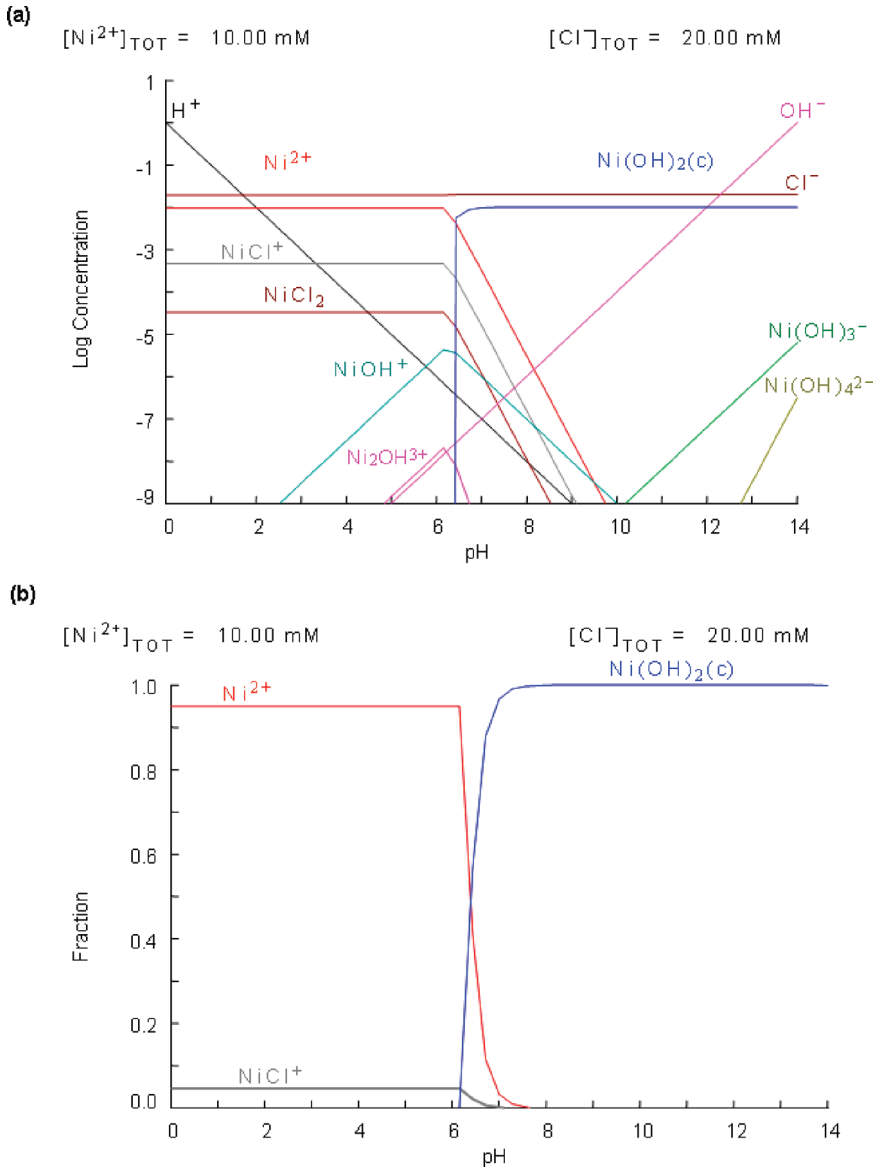

FIGURE 5. Thermodynamic modeling diagrams showing (a) the log concentration of all possible nickel species vs pH and (b) the distributions of the fraction nickel species vs pH.

major groove (18). This, in turn, suggests a balance between the tight binding of the DNA to the mica surface and a local flexibility, as could be expected from distributed "adhesion points", as might occur if the nickel ions were complexed tightly but not all of the available complexation sites on the crystal plane were occupied.

An important observation with respect to enzyme fidelity is that the frequency of double-stranded breaks observed at locations not corresponding to the enzyme recognition sequence was low, roughly 2% of the total cleavage. This level of nonspecific cleavage is indistinguishable from simple breakage because of the overstretching and drying observed in cases where no enzyme is applied. Therefore, we conclude that the Ni^{2+} ion does not induce significant nonspecific cleavage of surface-adsorbed DNA molecules, which is surprising because this infidelity can occur when restriction enzymes are used in solutions containing divalent cations other than the required Mg^{2+} cofactor. Given that all of the available sites on the bound molecules are not cleaved, it is possible that the Ni^{2+} ion inhibits the enzyme directly or that simply the DNA is bound so tightly to the surface in some places that the enzyme cannot access the double helix in the required conformation.

CONCLUSIONS

Here we have presented the first direct surface analysis of Ni^{2+}-treated mica used to bind DNA for single-molecule biochemical studies. Using ToF-SIMS, a highly sensitive surface analysis technique, we demonstrated that nickel ions in solution are exchanged with native K^+ ions on the mica surface, and this exchange is responsible for alteration of the mica surface properties that facilitate strong binding of DNA. Our thermodynamic simulation of nickel ion speciation reveals that the concentration of divalent cations in solution is a strong function of the pH in the pH range 6−8. This is important because current models of DNA/mica binding are driven by the solution concentration of the divalent species (5, 8), which our results show can vary

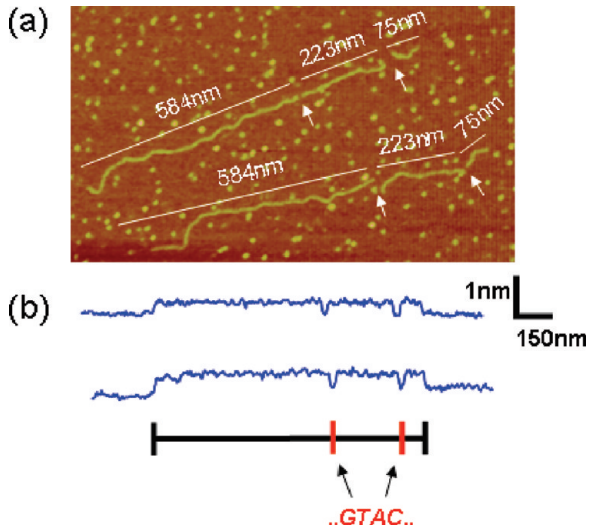

FIGURE 6. (a) Image of two pUC19 molecules on treated mica (10 mM $NiCl_2$) after in situ digestion with restriction enzyme *RsaI* (recognition sequence GATC). White arrows indicate gaps corresponding to the location of GTAC sequences within the DNA molecule. Fragment lengths (nm) are indicated on the image. (b) Corresponding height profile plots taken along the backbone contour of each molecule.

widely from what is assumed, and the speciation of other metal-ion complexes can be unpredictable unless great care is taken to stabilize the pH and redox conditions of the solution.

Using AFM, we detected a thin adlayer that forms when mica is treated with $NiCl_2$ solutions. The roughness imparted by this layer is not sensitive to the pH of the deposition solution, over the range pH 3.0−7.0. This layer can be difficult to distinguish from the bare mica surface itself. The results of the thermodynamic modeling, together with AFM and ToF-SIMS data, can be used for the selection of the optimum experimental conditions for the adsorption of Ni^{2+} from aqueous solutions onto the mica surface. In this way, it is possible to establish the chemical conditions (including pH, redox potential, concentration of the different ions used, etc.) as well as the boundary conditions in which Ni^{2+} ions could be adsorbed into the mica surface reproducibly.

Judged by the activity restriction enzymes, a reasonably robust 30−40% in situ cleavage efficiency with little to no nonspecific activity, $NiCl_2$ treatment not only provides a smooth, adhesive monolayer on mica capable of strongly adsorbing DNA but also provides a surface suitable for stable bioactivity. These results are comparable to those we have achieved on APTES-treated mica surfaces (17), which require more preparation time and have less reproducible roughness and DNA binding properties than does nickel/mica. On the basis of these results, we expect that DNA polymerases, which require similar levels of template molecule access and flexibility as restriction enzymes, would also function on molecules adsorbed to nickel/mica. Optical microscopy of in situ DNA polymerase activity on molecules fixed to modified glass substrates, using fluorescently labeled nucleotides and intercalating dyes as reporters is common and is a key step in the technologically important "next-gen" DNA-sequencing method. The use of "bioactive" nickel/mica substrates, instead of modified, relatively rough glass or silicon substrates, could open these important biochemical systems to investigation with scanning probe microscopies and their attendant advantages of spatial resolution and chemical/mechanical/electronic imaging modes.

METHODS

Mica and Silicon Substrates. Mica is a layered silicate of the general formula $K(Al_2)Si_3Al)O_{10}(OH)_2$, whose structure and properties have been reviewed elsewhere (19). Samples were prepared on freshly cleaved 9.9 mm V1 mica disks (Ted Pella, Inc.). Following cleavage, the mica was derivatized with 100 μL aliquots of 10, 8, 6, 4, and 2 mM $NiCl_2$ solutions for 10 s, rinsed with ultrapure water, and then dried with a stream of dry nitrogen. Samples measured with ToF-SIMS were derivatized with 10 mM $NiCl_2$ only. Silicon samples cut from a 100 mm silicon wafer (University Wafer) were cleaned in a heated 3:1 sulfuric acid and 30% hydrogen peroxide piranha solution, rinsed thoroughly with ultrapure water, and dried with dinitrogen. Silicon was derivatized with 100 μL aliquots of a 10 mM $NiCl_2$ solution, either blown dry with dry nitrogen or evaporated at room temperature, then rinsed with ultrapure water, and dried with a stream of dry nitrogen. All control samples, 0 mM $NiCl_2$ on mica and silicon, used ultrapure water in lieu of $NiCl_2$ solutions. All samples were stored in dry nitrogen-filled containers until time of measurement. $NiCl_2$ titrations of 10, 8, 6, 4, and 2 mM were made from a 0.5 M $NiCl_2$ stock solution of ultrapure water (pH 7.7−8.0) and anhydrous nickel(II) chloride (98% pure; Aldrich) and were then frozen in aliquots until time of use. The pH of the stock solutions was in the range of 6.58−6.61. Solutions are filtered before deposition onto substrates and applied in low humidity (~30% RH) at 22 °C in 100 μL aliquots. The pH of the 10 mM $NiCl_2$ solutions ranged from 7.65−7.73.

ToF-SIMS. The spectra were collected on a TRIFT II ToF-SIMS, using 22 keV of Au^+ primary ion over a 25 μm area. The samples were analyzed as received, no rinsing and no cleaning. For the untreated mica sample, mica was pealed from the backing glass; for the treated sample, the backing glass slice was cut to fit into the instrument.

AFM. AFM images were acquired with a Veeco Dimension 3000 atomic force microscope, in tapping mode, using manufacturer-supplied FESP cantilevers ($k = 3$ N m^{-1} and $f = 60$−100 kHz). Imaging was conducted at 22 °C and ~30% humidity. Images were acquired using linear scanning speeds of ~3−9 μm s^{-1} with an average resolution of 512 × 512 pixels per 2 × 2 μm area.

Thermodynamic Simulation of Ion Speciation. The modeling of the nickel species was performed using chemical equilibria and information on stability constants for all of the basic nickel chlorides included in the software *Make Equilibrium Diagrams Using Sophisticated Algorithms* (20, 21).

DNA Deposition and in Situ Enzymatic Digestion. Linear pUC19 DNA molecules were elongated and deposited onto derivatized mica surfaces using fluid flow (22). After DNA was elongated and immobilized on the derivatized mica surface, 100 μl aliquots of a buffer solution (10 mM Tris-HCl, pH 7.5 at 37 °C, 10 mM $MgCl_2$) containing two units of a *RsaI* restriction enzyme (recognition sequence GTAC) were deposited on mica samples and incubated at 37 °C in a humidified heater for 30 min to 1 h. The enzyme solution was then blown off with nitrogen, rinsed vigorously three times with ultrapure water, and dried with nitrogen. To quantify the digestion kinetics of the surface-bound DNAs, 40 representative, randomly selected AFM images, from five independently prepared substrates, containing 132 digested pUC19 molecules were scored for the number of specific and nonspecific cleaves, based on the known DNA sequence of the plasmid. Of a possible 264 specific

cleavage sites, 108 (41%) were successfully cleaved with 5 (2%) additional double-stranded breaks in locations not containing an enzyme recognition site.

Acknowledgment. This research was supported by NIH Grant R21 GM08099.

REFERENCES AND NOTES

(1) Hansma, H. G.; Laney, D. E. *Biophys. J.* **1996**, *70*, 1933–1939.
(2) Guthold, M.; Zhu, X. S.; Rivetti, C.; Yang, G. L.; Thomson, N. H.; Kasas, S.; Hansma, H. G.; Smith, B.; Hansma, P. K.; Bustamante, C. *Biophys. J.* **1999**, *77*, 2284–2294.
(3) McMaster, T. J.; Miles, M. J.; Shewry, P. R.; Tatham, A. S. *Langmuir* **2000**, *16*, 1463–1468.
(4) Pietrement, O.; Pastre, D.; Fusil, S.; Jeusset, J.; David, M. O.; Landousy, F.; Hamon, L.; Zozime, A.; Le Cam, E. *Langmuir* **2003**, *19*, 2536–2539.
(5) Sushko, M. L.; Shluger, A. L.; Rivetti, C. *Langmuir* **2006**, *22*, 7678–7688.
(6) Pastre, D.; Hamon, L.; Landousy, F.; Sorel, I.; David, M. O.; Zozime, A.; Le Cam, E.; Pietrement, O. *Langmuir* **2006**, *22*, 6651–6660.
(7) Cheng, H.; Zhang, K.; Libera, J. A.; de la Cruz, M. O.; Bedzyk, M. J. *Biophys. J.* **2006**, *90*, 1164–1174.
(8) Pastre, D.; Pietrement, O.; Fusil, P.; Landousy, F.; Jeusset, J.; David, M. O.; Hamon, C.; Le Cam, E.; Zozime, A. *Biophys. J.* **2003**, *85*, 2507–2518.
(9) Margulies, M.; Egholm, M.; Altman, W. E.; Attiya, S.; Bader, J. S.; Bemben, L. A.; Berka, J.; Braverman, M. S.; Chen, Y. J.; Chen, Z. T.; Dewell, S. B.; Du, L.; Fierro, J. M.; Gomes, X. V.; Godwin, B. C.; He, W.; Helgesen, S.; Ho, C. H.; Irzyk, G. P.; Jando, S. C.; Alenquer, M. L. I.; Jarvie, T. P.; Jirage, K. B.; Kim, J. B.; Knight, J. R.; Lanza, J. R.; Leamon, J. H.; Lefkowitz, S. M.; Lei, M.; Li, J.; Lohman, K. L.; Lu, H.; Makhijani, V. B.; McDade, K. E.; McKenna, M. P.; Myers, E. W.; Nickerson, E.; Nobile, J. R.; Plant, R.; Puc, B. P.; Ronan, M. T.; Roth, G. T.; Sarkis, G. J.; Simons, J. F.; Simpson, J. W.; Srinivasan, M.; Tartaro, K. R.; Tomasz, A.; Vogt, K. A.; Volkmer, G. A.; Wang, S. H.; Wang, Y.; Weiner, M. P.; Yu, P. G.; Begley, R. F.; Rothberg, J. M. *Nature* **2005**, *437*, 376–380.
(10) Holt, R. A.; Jones, S. J. M. *Genome Res.* **2008**, *18*, 839–846.
(11) Chee, M.; Yang, R.; Hubbell, E.; Berno, A.; Huang, X. C.; Stern, D.; Winkler, J.; Lockhart, D. J.; Morris, M. S.; Fodor, S. P. A. *Science* **1996**, *274*, 610–614.
(12) Oshannessy, D. J.; Brighamburke, M.; Peck, K. *Anal. Biochem.* **1992**, *205*, 132–136.
(13) Reed, J.; Hsueh, C.; Mishra, B.; Gimzewski, J. K. *Nanotechnology* **2008**, 19.
(14) Pashley, R. M.; Quirk, J. P. *Colloids Surf.* **1984**, *9*, 1–17.
(15) Pashley, R. M.; Israelachvili, J. N. *J. Colloid Interface Sci.* **1984**, *97*, 446–455.
(16) Burgess, J. *Metal ions in solution*; Halsted Press: New York, 1978; p 481.
(17) Reed, J.; Mishra, B.; Pittenger, B.; Magonov, S.; Troke, J.; Teitell, M. A.; Gimzewski, J. K. *Nanotechnology* **2007**, *18*, 044032(15 pp).
(18) Pingoud, A.; Fuxreiter, M.; Pingoud, V.; Wende, W. *Cell. Mol. Life Sci.* **2005**, *62*, 685–707.
(19) Radoslovich, E. W. *Acta Crystallogr.* **1960**, *13*, 919–932.
(20) Puigdomenech, I. *Abstr. Pap. Am. Chem. Soc.* **2000**, *219*, 248-IEC.
(21) Puigdomenech, I. *INPUT, SED, and PREDOM: Computer programs drawing equilibrium diagrams; TRITA-OOK-3010*; Department of Inorganic Chemistry, Royal Institute of Technology: Stockholm, Sweden, 1983; p 12 pp.
(22) Jing, J. P.; Reed, J.; Huang, J.; Hu, X. H.; Clarke, V.; Edington, J.; Housman, D.; Anantharaman, T. S.; Huff, E. J.; Mishra, B.; Porter, B.; Shenker, A.; Wolfson, E.; Hiort, C.; Kantor, R.; Aston, C.; Schwartz, D. C. *Proc. Natl. Acad. Sci. U.S.A.* **1998**, *95*, 8046–8051.

AM100697Z